Advanced Optical Modulators for Sub-THz-to-Optical Signal Conversion

Yuya Yamaguchi, *Member, IEEE*, Pham Tien Dat, *Member, IEEE*, Shingo Takano, Masayuki Motoya, Shotaro Hirata, Yu Kataoka, Junichiro Ichikawa, Ryo Shimizu, Naokatsu Yamamoto, Kouichi Akahane, Atsushi Kanno, *Senior Member, IEEE*, and Tetsuya Kawanishi, *Fellow, IEEE*

(Invited Paper)

***Abstract*—The use of sub-terahertz (sub-THz) and/or THz bands is a method of achieving some attractive applications such as future large-capacity radio over fiber (RoF) networks. However, in the current scenario, the performance of devices operating in the THz band is considerably worse than that of devices operating in the microwave band. An optical modulator is a device that converts electrical signals such as microwave, sub-THz, and THz signals to optical signals, and their conversion efficiency decreases when they are operated at higher frequencies. In this paper, we investigate two types of optical modulators. One is a long effective-length modulator to maximize its responsivity in the > 100 GHz range. It has an advantage for band-limited applications such as RoF. The other is a broadband modulator integrated with an electro-optic (EO) frequency-domain equalizer. The fabricated modulator achieved an over 110-GHz 3-dB bandwidth by customizing the optical circuit diagram in a traveling-wave modulator, and in a numerical estimation, the 3-dB bandwidth reached sub-THz. We also investigated the modulation distortions of the modulator with the equalizer. Using the measurement results, the optical crosstalk in the EO equalizer of the fabricated modulator was estimated to be less than −30 dB, and the distortion attributable to the EO equalizer in the modulator was sufficiently small to be negligible. We also measured a third-order intermodulation distortion, and the results showed that integration of the equalizer does not cause a degradation of modulation linearity. The obtained spurious-free dynamic range was as high as 83.3 dB.**

***Index Terms*—Optical modulator, Optical fiber communication, Radio over fiber, Lithium niobate, Modulation distortion**

This work was supported in part by JSPS KAKENHI Grant Number 22K04116, 23K13340, JST CREST Grant Number JPMJCR2103, and JST Moonshot R&D Program Grant Number JPMJMS226C.

(Corresponding author: Yuya Yamaguchi)

Y. Yamaguchi, P. T. Dat, N. Yamamoto and K. Akahane are with National Institute of Information and Communications Technology, Tokyo 184-8795, Japan (e-mail: yamaguchi@nict.go.jp ptdat@nict.go.jp, naokatsu@nict.go.jp, akahane@nict.go.jp).

S. Takano, M. Motoya, S. Hirata, Y. Kataoka, J. Ichikawa, and R. Shimizu are with Sumitomo Osaka Cement Co. Ltd., Chiba 274-8601, Japan (e-mail: stakano@soc.co.jp, mmotoya@soc.co.jp, shirata@soc.co.jp, ykataoka@soc.co.jp, jichikawa@soc.co.jp, rshimizu@soc.co.jp).

A. Kanno is with Nagoya Institute of Technology, Aichi 466-8555, Japan, and also with National Institute of Information and Communications Technology, Tokyo 184-8795, Japan (e-mail: kanno.atsushi@nitech.ac.jp).

T. Kawanishi is with Waseda University, Tokyo 169-8555, Japan, and also with National Institute of Information and Communications Technology, Tokyo 184-8795, Japan (e-mail: kawanishi@waseda.jp).

Color versions of one or more of the figures in this article are available online at http://ieeexplore.ieee.org

I. Introduction

High-speed optical modulators are key devices for high-baud-rate optical fiber communications. An increase in the baud rate has the potential to increase the total link capacity without increasing parallel multiplexing, such as wavelength-division multiplexing. Radio over fiber (RoF) technology is becoming popular as a key technology to connect radio networks to optical fiber networks seamlessly [1]. For future mobile networks, such as beyond 5G or 6G, the use of millimeter and terahertz (THz) waves will be a method of achieving a significantly large link capacity by utilizing their large bandwidth compared with the microwave band [2, 3]. Assuming this scenario, optical modulators that operate at millimeter-wave and/or THz frequencies with high responsivity are necessary for RoF links.

A high-speed modulator is essential for both digital coherent and RoF links; however, the required performance differs for these applications. For digital coherent links, a low half-wave voltage and large 3-dB bandwidth are required for baseband modulation. In contrast, a band-limited operation is sufficient for RoF links, but then a low half-wave voltage at the specified frequency is required for RoF applications. From this perspective, the difference in the required specifications means that the concept of device design is different for each application.

In this paper, we introduce a method for designing a lithium niobate (LN) modulator to optimize its electro-optic responsivity for RoF applications. Subsequently, a broadband modulator with a sub-THz 3-dB bandwidth is discussed, along with some experimental evaluations of its modulation linearity. Moreover, we investigate the potential of thin-film-type LN modulators for the sub-THz-to-optical signal conversion using electrical characterization.

II. Modulator Design Optimization for RoF Applications

Several types of high-speed optical modulators based on thin-film LN [4-12], InP [13-15], electro-optic polymer [16-18] have been reported. As an example of ultra-high-speed modulators, optical modulation at 500 GHz was demonstrated using an electro-optic-polymer-based plasmonic modulator

This article has been accepted for publication in IEEE Journal of Selected Topics in Quantum Electronics. This is the author's version which has not been fully edited and content may change prior to final publication. Citation information: DOI 10.1109/JSTQE.2023.3288275

and a thin-film LN modulator. The plasmonic modulator had an extremely large 3-dB bandwidth of 500 GHz and a low DC half-wave voltage of 3 V; however, the disadvantage of the structure is a large optical loss of > 20 dB in total [17]. Because the optical loss is critical to the total RF link gain, in general, the loss is needed to be smaller to obtain better link performance [19]. The 500-GHz modulation using a thin-film LN modulator was also reported, and its DC half-wave voltage was 3.8 V [6]. The 3-dB bandwidth of the modulator was approximately 50 GHz, and the half-wave voltage at 500 GHz was approximately 40 V. The pioneering demonstration of the optical modulation at THz frequency is cutting-edge; however, the drive voltage is needed to be smaller for industrial use for RoF applications. While the total optical loss of the modulator was 40 dB, a rib waveguide on a thin-film LN can achieve a low propagation loss because of its low absorption at telecom wavelengths. In a cutting-edge experimental demonstration, an ultra-low propagation loss of 0.002 dB/cm was reported [20]. The Ti-diffused waveguide on LN is a well-known and established technology, and the typical propagation loss is as low as 0.1 dB/cm. A characteristic of the Ti-diffused waveguide is that the optical mode size matches well with that of a single-mode fiber (SMF). Therefore, the typical butt-coupling loss between the Ti-diffused waveguide and SMF is as low as < 1 dB/facet, whereas the coupling loss between the tapered waveguide on the thin-film LN and lensed fiber is typically approximately 5 dB/facet [7].

For RoF links, the link gain is linear to the square of the slope efficiency of the modulator, and the slope efficiency, also called electro-optic (EO) responsivity, is defined as

$$s_{Mod} = \frac{\pi P_I T_{ff} R_s}{2V_\pi} \tag{1}$$

where P_I is the optical input power from a laser, T_{ff} is the fiber-to-fiber transmittance of the modulator (related to the total insertion loss), R_s is the impedance of the electrical source, and $V\pi$ is the half-wave voltage [19]. According to Eq. 1, an increase in the 3-dB optical loss of the modulator causes a 6-dB link gain reduction. Similarly, when the half-wave voltage of the modulator is doubled, the link gain is reduced by 6 dB. Thus, in addition to the half-wave voltage, the optical loss is a dominant parameter for the link gain of RoF links. Therefore, we developed a low-loss LN modulator to achieve a high link gain and obtain a high signal power at the receiver side for a high signal-to-noise ratio.

The modulator structure is shown in Fig. 1. The substrate was x-cut LN, and a Mach–Zehnder (MZ) interferometric optical waveguide was formed via the thermal diffusion of titanium. The propagation loss of the Ti-diffused waveguide was as low as 0.1 dB/cm. To improve the response in the high-frequency range, we applied a layered structure by mechanically polishing the backside of the device. A comparison of the cross-sectional structures of conventional bulk and layered substrates is shown in Fig. 2. The frequency response of a traveling-wave modulator is limited by velocity matching and electrical propagation loss. Velocity matching

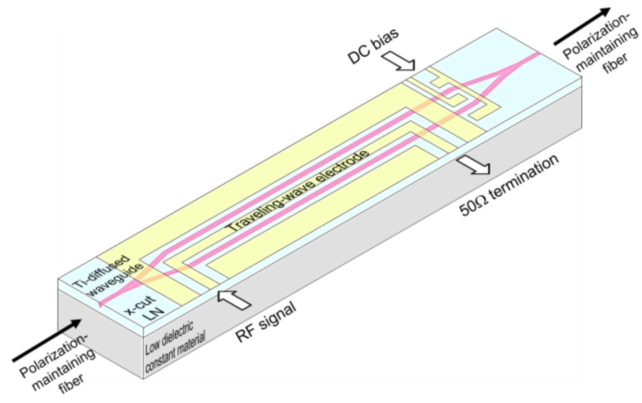

Fig. 1. Ti-diffused LN modulator with a layered substrate.

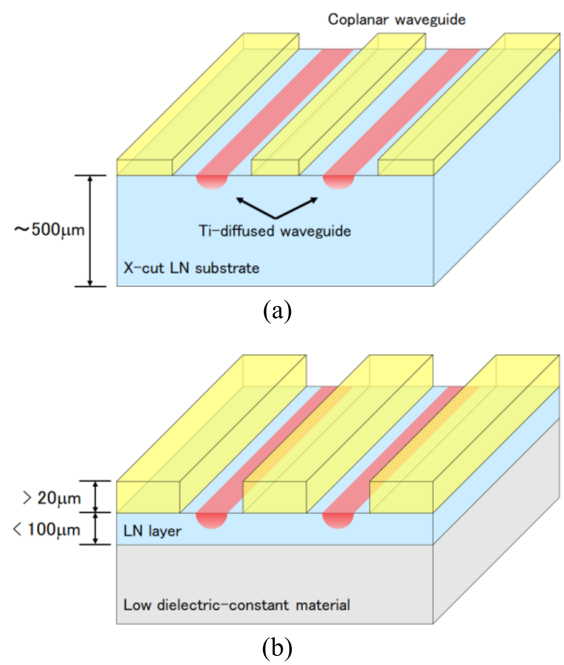

Fig. 2. Cross-structural comparison of the bulk substrate (a) and layered substrate (b).

can satisfy this condition by designing optical waveguides and electrode structures. The frequency response primarily depends on the electrical propagation loss. The electrical propagation loss can be expressed as the sum of the conduction and dielectric losses, and making the signal electrode wider and thicker reduces the conduction loss, particularly at high frequencies. However, the electrode structure is often limited by impedance matching to 50 **Ω**, and the electrode width and thickness are limited to being narrow and thin, respectively, owing to the high dielectric constant of LN. By applying a layered structure to the substrate, the material of the handle wafer is replaced with a low-dielectric-constant material such as SiO_2. Thereafter, we can design a coplanar waveguide with a wide and thick signal electrode

This article has been accepted for publication in IEEE Journal of Selected Topics in Quantum Electronics. This is the author's version which has not been fully edited and content may change prior to final publication. Citation information: DOI 10.1109/JSTQE.2023.3288275

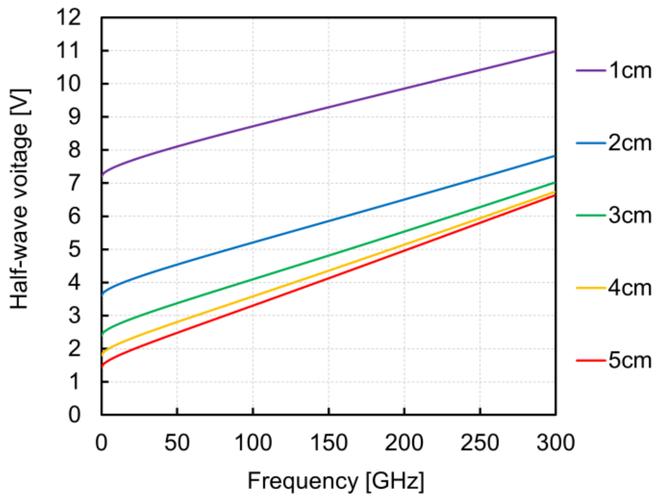

Fig. 3. Calculated frequency-dependent half-wave voltages of modulators with different effective lengths.

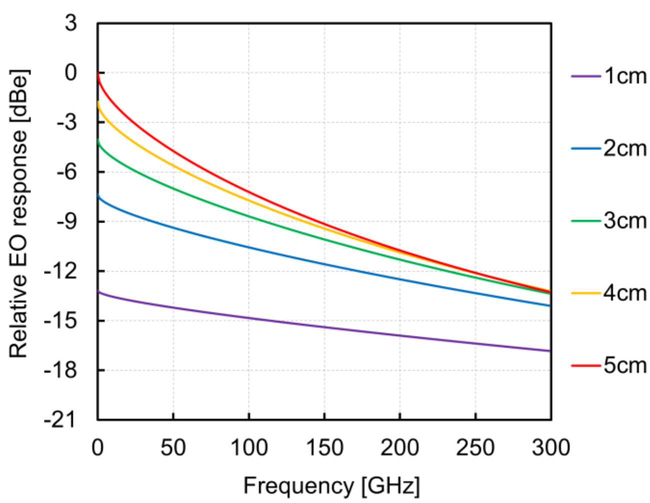

Fig. 4. Simulated relative EO response of modulators depending on the effective length.

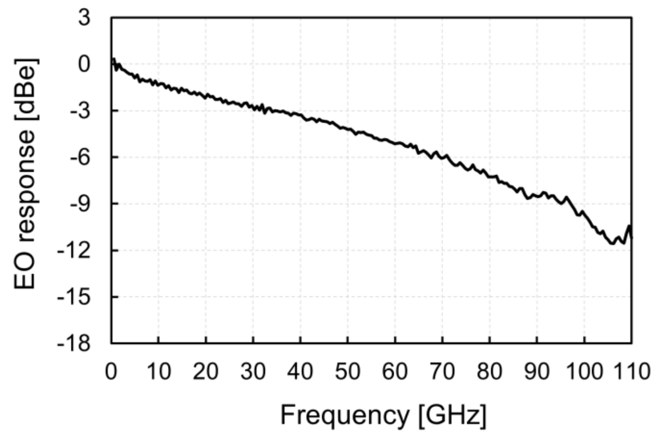

Fig. 5. Measured frequency response of the Ti-diffused LN modulator using layered substrate structure with a 5-cm effective length.

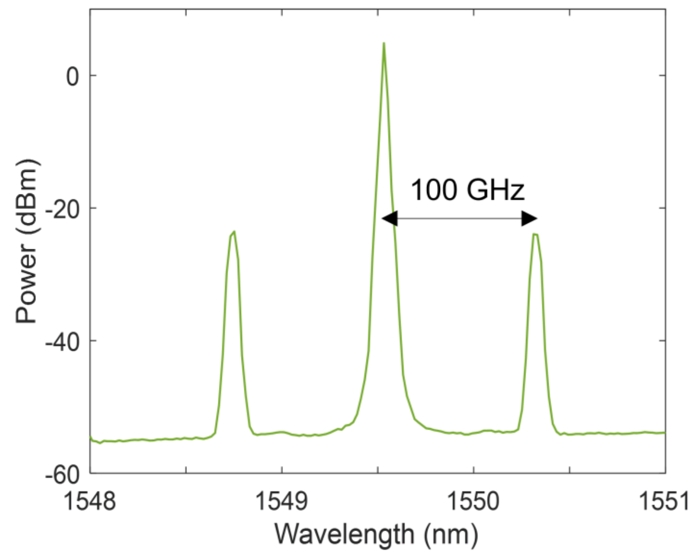

Fig. 6. Spectrum of optical signal modulated using a 5-GHz bandwidth 100-GHz carrier-frequency radio signal.

compared to the bulk case.

Next, we consider device-length optimization to obtain high EO responsivity for RoF applications. Here, we assume the cross-sectional structure of our previous study [21]. The measured DC half-wave voltage × effective length product is 7.2 V·cm. Here, the effective length is defined as a length of the modulation section where there is an interaction between the lightwaves and input voltage signals via Pockels effect. The calculated frequency-dependent half-wave voltages under several effective-length conditions are shown in Fig. 3. The DC half-wave voltage decreases linearly with respect to the inverse of the effective length. Therefore, it is well known that designing a modulator with a longer effective length is a reasonable method of decreasing the half-wave voltage at low frequencies. While the flatness of the frequency response is degraded, a longer device has an advantage in terms of the half-wave voltage at any frequency, as shown in Fig. 3. The simulated relative EO responses of the modulators depending on the effective length, where the optical and electrical propagation losses are taken from [21], are shown in Fig. 4. The simulated results include the response degradation attributable from an optical propagation loss of 0.1 dB/cm, and the EO responsivities are normalized by that of the 5 cm case. In our cross-sectional design, a 5-cm effective length has a higher EO responsivity than shorter devices in the frequency range of DC to 250 GHz although the 3-dB bandwidth of the 5-cm device is only 25 GHz. Thus, a modulator with a very long effective length has an advantage in terms of the total EO responsivity for band-limited modulation, such as RoF applications [22].

The frequency response of our latest product is shown in Fig. 5. The effective length was 5 cm, and the DC half-wave

This article has been accepted for publication in IEEE Journal of Selected Topics in Quantum Electronics. This is the author's version which has not been fully edited and content may change prior to final publication. Citation information: DOI 10.1109/JSTQE.2023.3288275

voltage was 1.5 V. The measured 3-dB bandwidth was approximately 30 GHz, and the response curve exhibited a smoothly degraded response up to 110 GHz. Although the EO response at 100 GHz was about -10 dB in this long effective-length modulator, the relative EO responsivity at 100 GHz was estimated to be higher than that of shorter modulators. The insertion loss, as the sum of the fiber-coupling and propagation losses of the fabricated modulator, was as low as 4 dB using a Ti-diffused waveguide. We confirmed modulator operation in the high-frequency range. The spectrum of the optical signal modulated using a 5-GHz bandwidth 100-GHz carrier-frequency radio signal for RoF transmission is shown in Fig. 6. The driving signal power was around −2dBm. The modulation sideband was clearly observed owing to its high EO responsivity.

III. Broadband Modulator with Electro-Optic Frequency-Domain Equalizer

While a band-limited electrical signal is used in RoF links, baseband operation and a large 3-dB bandwidth are required for optical fiber communication. In this section, we review an EO frequency-domain equalizer that can enlarge the 3-dB bandwidth of conventional traveling-wave modulators [23].

The traveling-wave electrode is a typical structure for high-speed optical modulation. While the operatable frequency is limited by the RC time constant in lumped-electrode-type modulators, traveling-wave modulators are not limited by such restrictions [24]. However, the 3-dB bandwidth of traveling-wave modulators is limited by velocity matching and electrical propagation loss, as indicated in Sec. II. Generally, optical waveguides and electrodes are designed to achieve the velocity-matching condition. To achieve the velocity matching without efficiency degradation, some methods to design the modulation polarity or phase with unique structure such as meander electrodes, meander optical waveguides, polarization reversal of ferroelectric crystal [25-29]. Under the velocity matching condition, the 3-dB bandwidth of the traveling-wave modulator is limited by the electrical propagation loss, which is larger at higher frequencies. To create a higher-bandwidth modulator by relaxing the restrictions, we propose an EO equalizer.

The structure of the traveling-wave modulator integrated with the EO equalizer is shown in Fig. 7. The modulator consists of a fundamental modulation section, same-polarity modulation section, waveguide-crossing section, and reverse-polarity modulation section. The length of each section is defined as L, rL, sL, and rL, respectively. To evaluate the numerical advantage of the EO equalizer, we define the relative EO response improvement R_{Eq} as follows:

$$R_{Eq} \equiv \left|\frac{\phi_{MZ\ with\ Eq}}{\phi_{MZ}}\right|^2$$

$$= \left|\frac{\int_0^{L(1+r)} V(x)\,dx - \int_{L(1+r+s)}^{L(1+2r+s)} V(x)\,dx}{\int_0^{L} V(x)\,dx}\right|^2 \qquad (2)$$

where $V(x)$ is the voltage after a propagation length of x. For the traveling-wave electrode, $V(x)$ can be described as

$$V(x) = V_0 \exp\left\{-\left(\alpha_c\sqrt{f} + \alpha_d f\right)x\right\} \qquad (3)$$

where V_0 is the input voltage, α_c is a constant for the conduction loss, α_d is a constant for the dielectric loss, and f is the frequency of the modulation signal. $R_{Eq} = 1$ when $f = 0$, which means that there is no improvement in the DC EO response. In contrast, $R_{Eq} > 1$ when $f > 0$; therefore, the responsivity at a high frequency is improved by the integration of the EO equalizer. The numerical calculations of the frequency response of the modulator with and without the EO equalizer are shown in Fig. 8, where $L = 1.9$ cm, $r = 1$, and $s = 1.4$. The electrical loss parameter was set to the same value as in our previous study [9]. While the 3-dB bandwidth of a 1.9-cm modulator without the equalizer was approximately 100 GHz, that of a modulator with an EO equalizer reached 200 GHz under the same DC half-wave voltage. Thus, the 3-dB bandwidth of the modulator can be approximately doubled by integrating the EO equalizer.

For the experimental demonstration, we fabricated an LN

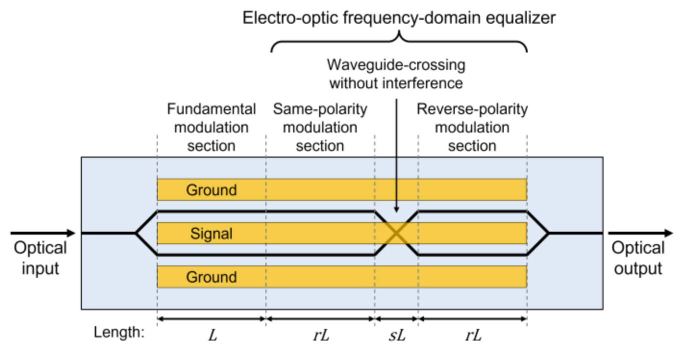

Fig. 7. A structure of travelling-wave modulator integrated with electro-optic frequency-domain equalizer.

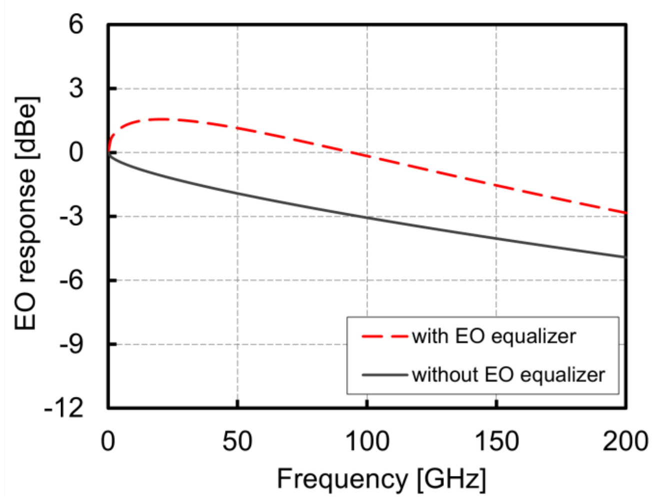

Fig. 8. Calculated frequency response of the modulator with and without the EO equalizer ($r = 1$, $s = 1.4$).

This article has been accepted for publication in IEEE Journal of Selected Topics in Quantum Electronics. This is the author's version which has not been fully edited and content may change prior to final publication. Citation information: DOI 10.1109/JSTQE.2023.3288275

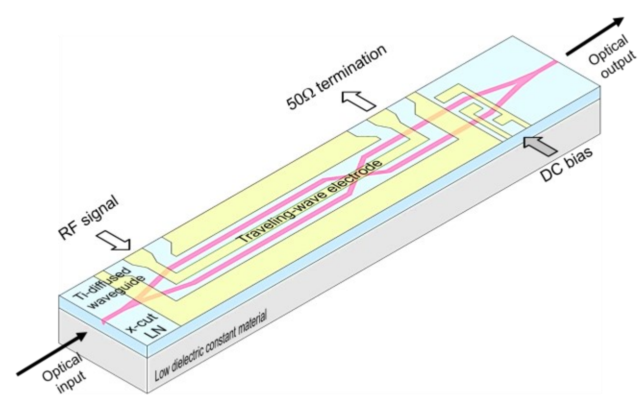

Fig. 9. Ti-diffused LN modulator integrated with EO equalizer.

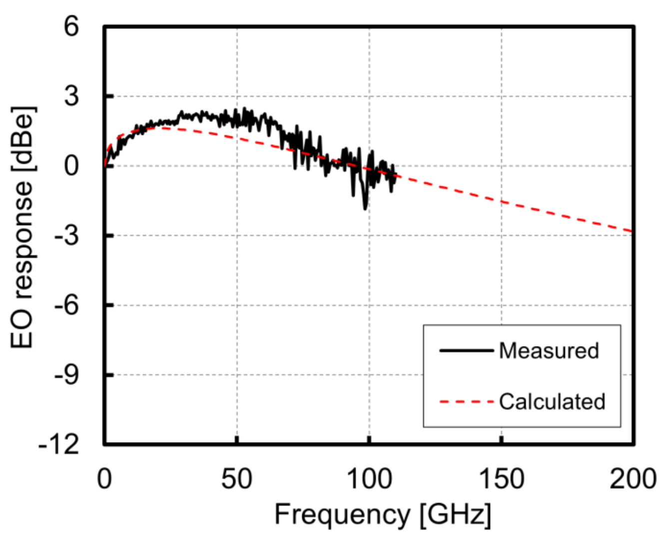

Fig. 10. Measured frequency response of the LN modulator with EO equalizer.

modulator with an EO equalizer, as shown in Fig. 9. The optical waveguides were formed via the thermal diffusion of titanium, and the electrodes were formed via gold electroplating. The optical waveguides included a crossing structure for an EO equalizer. The LN substrate was thinned by polishing its backside to improve its electrical characteristics at high frequencies. The fundamental modulation length L was 1.9 cm, and the total electrode length of the modulator was 8.4 cm, including the EO equalizer sections of r = 1 and s = 1.4. Although the device was large owing to the integration of the EO equalizer, the optical insertion loss consisting of the propagation loss and fiber-coupling loss was as small as 5.4 dB. The DC half-wave voltage was 3.7 V. The measured EO responses are shown in Fig. 10. The 3-dB bandwidth was greater than 110 GHz, which was the upper limit of our measurement setup. The measured value matched well with the calculated

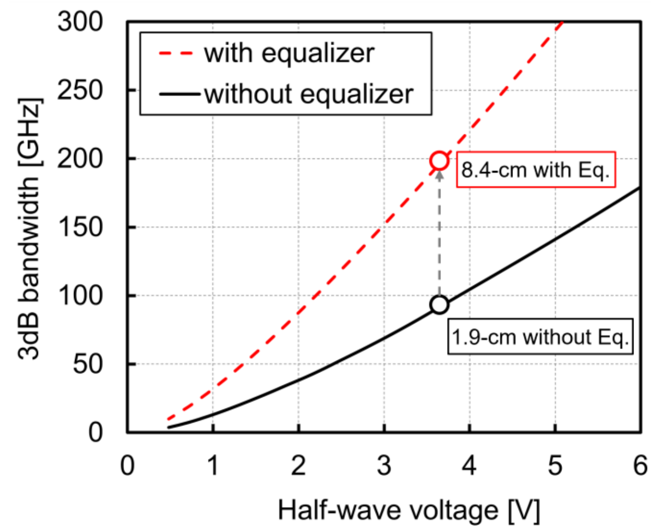

Fig. 11. Numerical calculation of an improvement of achievable specification of the modulator with the same cross-sectional structure by integrating the EO equalizer (r = 1, s = 1.4).

performance, and the 3-dB bandwidth was estimated to be approximately 200 GHz. We quantitively investigated the advantages of the EO equalizer, and the numerical calculation of the improvement of the achievable specification of our modulator structure by integrating the EO equalizer is shown in Fig. 11. This shows that the equalizer can approximately double the 3-dB bandwidth of the modulator while maintaining the same DC half-wave voltage. In the calculations, we assumed that the equalizer parameters were r = 1 and s = 1.4. Although there is a disadvantage in that the modulation length becomes almost three times larger compared with a conventional one, the bandwidth can be improved beyond the limitation determined by the modulator's cross-sectional structure. For future research, we propose a bending-waveguide-type EO equalizer for thin-film LN platforms, which has the potential to achieve a small device size even when the equalizer is integrated [23].

IV. Linearity Evaluation of the Modulator

The EO equalizer has an advantage of bandwidth enhancement; however, as a disadvantage of the crossing-waveguide-type EO equalizer, an increase in modulation distortion can be attributed to optical crosstalk at the waveguide-crossing section. Furthermore, determining the types of modulation distortions induced by optical crosstalk is difficult. In this study, we investigated the relationship between the modulation distortions and optical crosstalk at waveguide crossings using an EO equalizer.

A. Semi-Static Characteristics

The optical circuit of the MZ modulator with an EO equalizer was modeled as shown in Fig. 12. It consisted of a fundamental modulation section, same-polarity modulation section, waveguide crossing section, reverse-polarity modulation section, and bias control section. To simplify the model, we assumed that

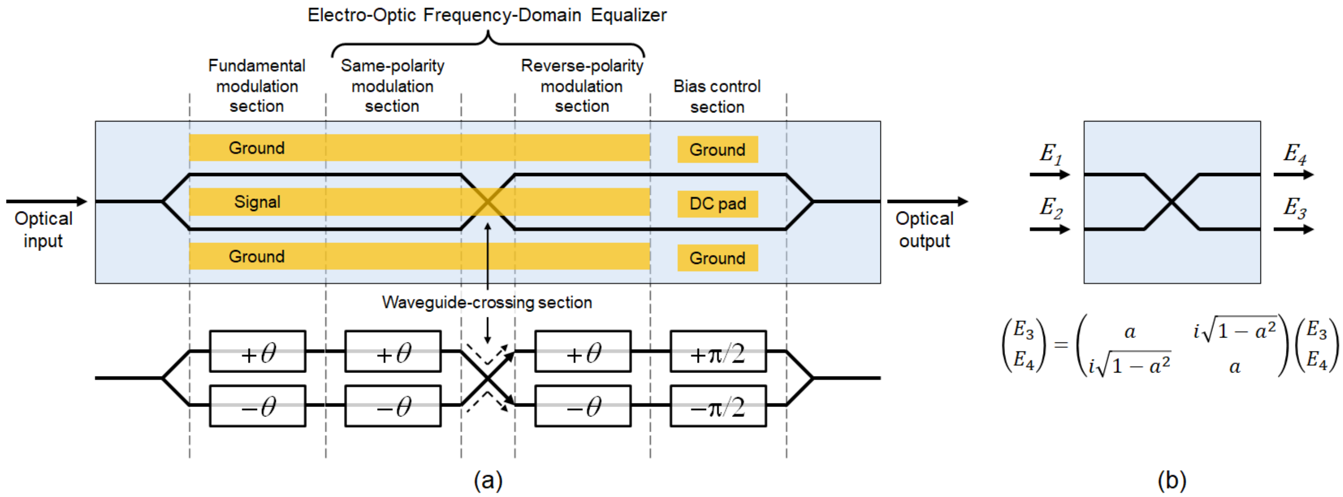

Fig. 12. (a) Optical circuit of MZ modulator integrated with an EO equalizer; (b) transfer matrix of crossing-waveguide.

the effective length and amount of the induced optical phase changes were the same in the fundamental modulation, same-polarity modulation, and reverse-polarity modulation sections. The modulator had a crossing waveguide for the EO equalizer, and the optical crosstalk at the waveguide crossing section could modulate the distortions.

For the mathematical expansion, we define the transfer matrix based on the symmetric-direction coupler model as follows:

$$\begin{pmatrix} E_3 \\ E_4 \end{pmatrix} = \begin{pmatrix} a & i\sqrt{1-a^2} \\ i\sqrt{1-a^2} & a \end{pmatrix} \begin{pmatrix} E_1 \\ E_2 \end{pmatrix} \tag{4}$$

where E_1, E_2, E_3, and E_4 are the electric fields at the input and output of the crossing waveguide, respectively, and a is the transmittance in the electric field domain. The output from the MZ modulator with the EO equalizer under the null bias condition is described as follows:

$$E_{out} = E_0 \left\{ \frac{a}{2} cos\left(\omega t + \theta - \frac{\pi}{2}\right) + \frac{a}{2} cos\left(\omega t - \theta + \frac{\pi}{2}\right) + \frac{i\sqrt{1-a^2}}{2} cos\left(\omega t + 3\theta + \frac{\pi}{2}\right) + \frac{i\sqrt{1-a^2}}{2} cos\left(\omega t - 3\theta - \frac{\pi}{2}\right) \right\}$$

$$= E_0 \left\{ a \cdot \cos(\omega t) \cdot \sin\theta + \sqrt{1-a^2} \cdot \sin(\omega t) \cdot \sin 3\theta \right\} \tag{5}$$

where $E_0 \cos(\omega t)$ is an input lightwave, and θ is the induced optical phase change at each section, as shown in Fig. 12. The equation indicates that the optical crosstalk component has thrice the phase changes of the desired signal response, and the distortion component has a $\sin 3\theta$ function, whereas the signal component has a $\sin\theta$ function related to the fundamental induced phase changes of θ. The calculated modulation curves for various crosstalk conditions are shown in Fig. 13 (a), where the optical crosstalk was defined as $10\log_{10}(1-a^2)$.

As the optical crosstalk increased, the modulation curve deviated from the theoretical sinusoidal response. To evaluate this distortion, we measured the modulation curve using the fabricated modulator. The measured results are shown in Fig. 13 (b) and (c) on linear and logarithmic scales, respectively. We measured the data for two cases: applying a voltage to the traveling-wave electrode and applying a voltage to the DC-bias electrode as a reference because the curve in the latter case should be sinusoidal regardless of the optical crosstalk at the EO equalizer. The two measured curves, shown in Fig. 13 (b), were nearly identical, and they were in good agreement with the theoretical calculations for a −30 dB optical crosstalk.

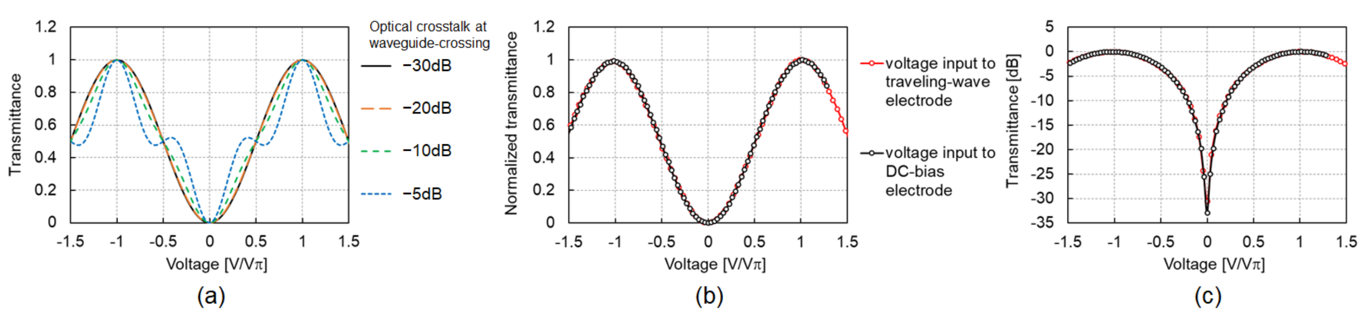

Fig. 13. (a) Calculated modulation curve under various optical crosstalk conditions; (b) measured modulation curve of the fabricated modulator on a linear scale; (c) modulation curve on a logarithmic scale.

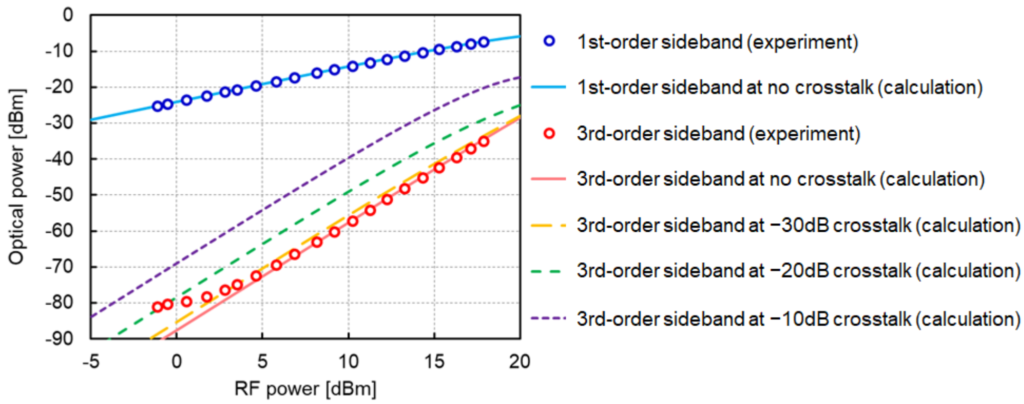

Fig. 14. Measured and calculated optical power of 1st- and 3rd-order modulation sidebands.

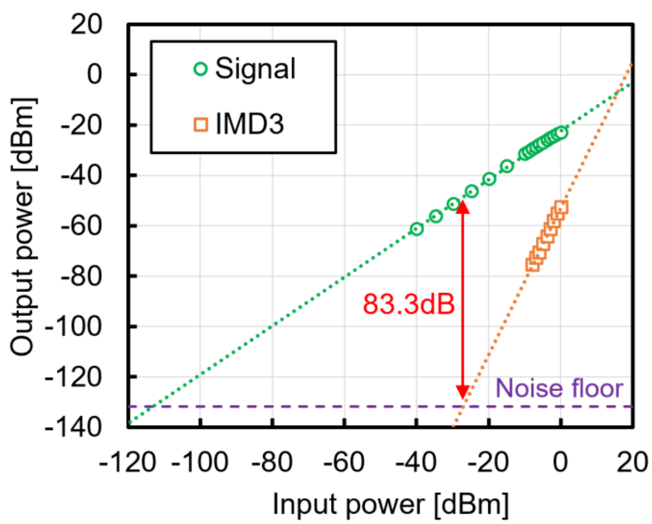

Fig. 15. Measured output RF power of signal and IMD3 components depending on an input RF power.

Moreover, the measured extinction ratio of the modulator was > 30 dB at the voltage input to the traveling-wave electrode, and the EO equalizer did not increase the distortion of the modulation curve of the fabricated modulator.

B. Dynamic Characteristics

For quantitative analysis of the modulation distortions, we measured the modulation spectrum under 10-GHz single-tone double-sideband suppressed-carrier (DSB-SC) modulation. The modulated optical component attributable to the optical crosstalk exhibited optical phase changes three times those of the desired signal component. Thus, the third-order modulation sideband related to the third-order nonlinearity of the MZ modulators increased dramatically in the lower RF driving power region, whereas the first-order modulation sideband increased linearly with the input RF power. By utilizing this relationship, we could estimate the crosstalk component although the optical power was considerably smaller than that of the signal component. The measured results and theoretical calculations for various optical-crosstalk conditions are shown in Fig. 14. The first-order sideband increased linearly with the input RF power, as expected from theory. As expected, the third-order sideband increased cubically with the RF power, and the power level was as small as the theoretical limitation of the MZ modulator. From the experiment, the optical crosstalk in the fabricated modulator was estimated to be smaller than −30 dB, and the distortion due to the crosstalk was sufficiently small to be negligible.

We also measured a third-order intermodulation distortion (IMD3) to evaluate the linearity of the fabricated modulator shown in Fig. 8. The optical input was 10 dBm at 1550 nm from a continuous wave laser, and the modulator was driven by a two-tone RF signal whose frequency was 10 GHz ± 5 MHz under the quadrature bias condition. The modulated optical signal was converted into an RF signal using a broadband photodiode (Fraunhofer HHI). The measured results are shown in Fig. 15. Similar to the prediction from the theory of MZ modulators, the output RF power of the signal and IMD3 components increased linearly and cubically with respect to the input RF power. The noise floor of our setup was estimated as -131.8 dBm/Hz, and then, the spurious-free dynamic range (SFDR) was calculated as 83.3 dB/Hz$^{2/3}$.

V. Conclusion

We investigated two types of modulator designs. One was for band-limited applications such as RoF and the other for broadband applications such as optical fiber communications. We observed that increasing the modulation length induces an increase in the EO responsivity, which is equivalent to a decrease in the half-wave voltage, even at high frequencies, such as in the sub-THz range. To achieve an optical modulator with a sub-THz 3-dB bandwidth, we proposed and demonstrated a traveling-wave modulator integrated with an EO equalizer. The fabricated modulator exhibited a > 110 GHz 3-dB bandwidth, a low optical insertion loss of 5.4 dB, and a low half-wave voltage of 3.7 V. As the research and development of high-speed modulators for optical fiber communications progresses, we expect that modulators capable of converting sub-THz (or THz) and optical signals with higher efficiency will be developed.

References

[1] T. Kawanishi, “THz and Photonic Seamless Communications,” *J. Lightw. Technol.*, vol. 37, no. 7, pp. 1671–1679, Feb. 2019.

This article has been accepted for publication in IEEE Journal of Selected Topics in Quantum Electronics. This is the author's version which has not been fully edited and content may change prior to final publication. Citation information: DOI 10.1109/JSTQE.2023.3288275

[2] A. J. Seeds, H. Shams, M. J. Fice, and C. C. Renaud, "TeraHertz Photonics for Wireless Communications," *Journal of Lightwave Technology*, vol. 33, no. 3, pp. 579–587, Feb. 2015.

[3] T. Nagatsuma, G. Ducournau, and C. C. Renaud, "Advances in terahertz communications accelerated by photonics," *Nature Photonics*, vol. 10, pp. 371-379, May 2016.

[4] V. E. Stenger, J. E. Toney, J. Scholl, J. Busch, A. Pollick,, P. Pontius, and S. Sriram, "Wide-Band Electro-Optic Modulator in Thin-Film Lithium Niobate on Quartz Substrate," *in Proc. European Conference on Optical Communication*, Sep. 2012, Tu.3.E.4.

[5] V. E. Stenger, J. E. Toney, J. Scholl, J. Busch, A. Pollick,, P. Pontius, and S. Sriram, "Low Loss and Low Vpi Thin Film Lithium Niobate on Quartz Electro-optic Modulators," *in Proc. European Conference on Optical Communication*, Sep. 2017, Tu.2.C.5.

[6] A. J. Marcante, S. Shi, P. Yao, L. Xie, R. M. Weikle, and D. W. Prather, "Thin film lithium niobate electro-optic modulator with terahertz operating bandwidth," *Optics Express*, vol. 26, no. 11, pp. 14810-14816, May 2018.

[7] C. Wang, M. Zhang, X. Chen, M. Bertrand, A. Shams-Ansari, S. Chandrasekhar, P. Winzer, and M. Loncar, "Integrated lithium niobate electro-optic modulators operating at CMOS-compatible voltages," *Nature*, vol. 562, pp. 101-104, Sep. 2018.

[8] M. Xu, M. He, H. Zhang, J. Jian, Y. Pan, X. Liu, L. Chen, X. Meng, H. Chen, Z. Li, X. Xiao, S. Yu, S. Yu, and X. Cai, "High-performance coherent optical modulators based on thin-film lithium niobate platform," *Nature Communications*, vol. 11, pp. 3911, Aug. 2020.

[9] P. Kharel, C. Reimer, K. Luke, L. He, and M. Zhang, "Breaking voltage–bandwidth limits in integrated lithium niobate modulators using micro-structured electrodes." *Optica*, vol. 8, pp. 357-363, Mar. 2021.

[10] M. Xu, Y. Zhu, F.Pittala, J. Tang, M. He, W. C. Ng, J. Wang, Z. Ruan, X. Tang, M. Kuschnerov, L. Liu, S. Yu, B. Zheng and X. Cai, "Dual-polarization thin-film lithium niobate in-phase quadrature modulators for terabit-per-second transmission." *Optica*, vol. 9, pp. 61-62, Jan. 2022.

[11] X. Wang, C. Shang, A. Pan, X. Cheng, T. Gui, S. Yuan, C. Gui, K. Zheng, P. Zhang, X. Song, Y. Li, L. Li, C. Zeng, and J. Xia, "Thin-film lithium niobate dual-polarization IQ modulator on a silicon substrate for single-carrier 1.6 Tb/s transmission," *APL Photonics*, vol. 7, pp. 076101, Jul. 2022.

[12] Y. Zhang, L. Shao, J. Yang, Z. Chen, K. Zhang, K. Shum, D. Zhu, C. H. Chan, M. Loncar, and C. Wang, "Systematic investigation of millimeter-wave optic modulation performance in thin-film lithium niobate," *Photonics Research*, vol. 10, pp. 2380-2387, Sep. 2022.

[13] H. Yagi, Y. Yoneda, M. Ekawa, and H. Shoji, "InP-based monolithic integration technologies for 100/200 Gb/s pluggable coherent transceivers," *IEICE Transactions on Electronics*, vol. E100-C, pp. 179-186, Feb 2017.

[14] S. Lange, S. Wolf, J. Lutz, L. Altenhain, R. Schmid, R. Kaiser, M. Schell, C. Koos, and S. Randel, "100 GBd Intensity Modulation and Direct Detection With an InP-Based Monolithic DFB Laser Mach–Zehnder Modulator," *Journal of Lightwave Technology*, vol. 36, pp. 97-102, Jan. 2018.

[15] J. Ozaki, Y. Ogiso, Y. Hashizume, H. Yamazaki, K. Nagashima, and M. Ishikawa, "Class-80 InP-based high-bandwidth coherent driver modulator with flexible printed circuit RF interface," *in Proc. European Conference on Optical Communication*, Sep. 2022, Mo.4F.1.

[16] H. Huang, S. R. Nuccio, Y. Yue, J. Y. Yang, Y. Ren, C. Wei, G. Yu, R. Dinu, D. Parekh, C. J. Chang-Hasnain, and A. E. Willner, "Broadband Modulation Performance of 100-GHz EO Polymer MZMs," *Journal of Lightwave Technology*, vol. 30, pp. 3647-3652, Dec. 2012.

[17] M. Burla, C Hoessbacher, W. Heni, C. Haffner, Y. Fedoryshyn, D. Werner, T. Watanabe, H. Massler, D. L. Elder, L. R. Dalton, and J. Leuthold, "500 GHz plasmonic Mach-Zehnder modulator enabling sub-THz microwave photonics," *APL Photonics*, vol. 4, pp. 056106, May 2019.

[18] C. Eschenbaum, A. Mertens, C. Fullner, A. Kuzmin, A. Schwarzenberger, A. Kotz, G. Ramann, M. Chen, J. Drisko, B. Johnson, J. Zyskind, J. Marcelli, M. Lebby, W. Freude, S. Randel, and C. Koos, "Thermally Stable Silicon-Organic Hybrid (SOH) Mach-Zehnder Modulator for 140 GBd PAM4 transmission with Sub-1 V Drive Signals," *in Proc. European Conference on Optical Communication*, Sep. 2022, Th3B.2.

[19] C. H. Cox, E. I. Ackerman, G. E. Betts, and J. L. Prince, "Limits on the Performance of RF-Over-Fiber Links and Their Impact on Device Design," *IEEE Transactions on Microwave Theory and Techniques*, vol. 54, no. 2, pp. 906-920, Feb. 2006.

[20] A. Shams-Ansari, G Huang, L. He, Z. Li, J. Holzgrafe, M. Jankowski, M. Churaev, P. Kharel, R. Cheng, D. Zhu, N. Sinclair, B. Desiatov, M. Zhang, T. J. Kippenberg, and M. Loncar, "Reduced material loss in thin-film lithium niobate waveguides," *APL Photonics*, vol. 7, pp. 081301, June 2022.

[21] Y. Yamaguchi, A. Kanno, N. Yamamoto, T. Kawanishi, and H. Nakajima, "High Extinction Ratio LN Modulator with Low Half-Wave Voltage and Small Chirp by Using Thin Substrate," *in Proc. Microoptics conference*, Oct. 2017, A-2.

[22] P. T. Dat, Y. Yamaguchi, M. Motoya, S. Oikawa, J. Ichikawa, A. Kanno, N. Yamamoto, and T. Kawanishi, "Transparent Fiber-Millimeter-Wave-Fiber System in 100-GHz Band Using Optical Modulator and Photonic Down-Conversion," *Journal of Lightwave Technology*, vol. 40, no. 5, pp. 1483–1493, Mar. 2022.

[23] Y. Yamaguchi. P. T. Dat, S. Takano, M. Motoya, Y. Kataoka, J. Ichikawa, S. Oikawa, R. Shimizu, N. Yamamoto, A. Kanno, and T. Kawanishi, "Low-Loss Ti-diffused LiNbO3 Modulator Integrated with Electro-Optic Frequency-Domain Equalizer for High Bandwidth Exceeding 110 GHz," *in Proc. European Conference on Optical Communication*, Sep. 2022, Tu4E.2.

[24] M. Izutsu, Y. Yamane, and T. Sueta, "Broad-band traveling-wave modulator using a LiNbO3 optical waveguide," *Journal of Quantum Electronics*, vol. 13, no. 4, pp. 287–290, Apr 1977.

[25] R. Alferness, S. K. Korotky, and E. A. J. Marcatili, "Velocity-Matching Techniques for Integrated Optic Traveling Wave Switch/Modulators," *Journal of Quantum Electronics*, vol. QE-20, no. 3, pp. 301–309, Mar. 1984.

[26] Y. Hinakura, D. Akiyama, H. Ito, and T. Baba, "Silicon Photonic Crystal Modulators for High-Speed Transmission and Wavelength Division Multiplexing," *Journal of Selected Topics in Quantum Electronics*, vol.27, no. 3, pp. 4900108, May/Jun. 2021.

[27] K.Aoki, J. Kondo, Y. Iwata, A. Hamajima, T. Ejiri, O. Mitomi, and M. Minakata, "High-Speed X-cut Thin-Sheet $LiNbO_3$ Optical Modulator With Folded Structure," *Journal of Lightwave Technology*, vol. 25, no. 7, pp. 1805–1810, Jul. 2007.

[28] P. Dong, J. H. Sinsky, and C. Gui, "Coplanar-waveguide-based silicon Mach–Zehnder modulator using a meandering optical waveguide and alternating-side PN junction loading," *Optics Letters*, vol. 41, no. 18, pp. 4401–4404, Sep. 2016.

[29] H. V. Pham, H. Murata and Y. Okamura, "Electrooptic Modulators with Controlled Frequency Responses by Using Nonperiodically Polarization-Reversed Structure," *Advances in OptoElectronics*, vol. 2008, pp. 948294, Sep. 2008.

Yuya Yamaguchi (Member, IEEE) received the B.E., M.E., and Ph.D. degrees in applied physics from Waseda University, Tokyo, Japan, in 2012, 2014, and 2017, respectively.

From 2015 to 2016, he was a research associate in Waseda University. Since 2016, he has been with the National Institute of Information and Communications Technology (NICT), Tokyo, Japan. His research interests include optical modulators and functional optoelectronic devices.

Dr. Yamaguchi is a member of the Institute of Electronics, Information, and Communication Engineers of Japan, and the Japan Society of Applied Physics.

Pham Tien Dat (Member, IEEE) received the B.Eng. degree in electronics and telecommunication engineering from the Posts and Telecommunications Institute of Technology, Hanoi, Vietnam, in 2003, and the M.Sc. and Ph.D. degrees in science from Waseda University, Tokyo, Japan, in 2008 and 2011, respectively.

In 2011, he joined the National Institute of Information and Communications Technology, Tokyo, Japan, where he is currently a Senior Researcher. His research interests include microwave/millimeter-wave photonics, radio over fiber,

This article has been accepted for publication in IEEE Journal of Selected Topics in Quantum Electronics. This is the author's version which has not been fully edited and content may change prior to final publication. Citation information: DOI 10.1109/JSTQE.2023.3288275

optical wireless systems, and seamless access networks for 5G and beyond.

Shingo Takano received the B.E. and M.E. degrees in electronics from Nagaoka University of Technology, Niigata, Japan, in 1998 and 2000, respectively.

In 2000, he joined Optoelectronics Research Division, New Technology Research Laboratories, Sumitomo Osaka Cement Co., Ltd., Chiba, Japan. He has been engaged in research and development of optical modulators.

Masayuki Motoya received the B.E. and M.E. degrees in science and technology from Nihon University, Tokyo, Japan, in 2004 and 2006, respectively.

In 2006, he joined Optoelectronics Research Division, New Technology Research Laboratories, Sumitomo Osaka Cement Co., Ltd., Chiba, Japan. He has been engaged in research and development of optical modulators.

Shotaro Hirata received the B.E. and M.E. degrees in applied chemistry from Osaka City University, Osaka, Japan, in 2016 and 2018, respectively.

In 2018, he joined Optoelectronics Research Division, New Technology Research Laboratories, Sumitomo Osaka Cement Co., Ltd., Chiba, Japan. He has been engaged in research and development of optical modulators.

Yu Kataoka received the B.E. and M.E. degrees in Chemistry and Materials Technology from Kyoto Institute of Technology, Kyoto, Japan, in 2013 and 2015, respectively.

In 2015, he joined Optoelectronics Research Division, New Technology Research Laboratories, Sumitomo Osaka Cement Co., Ltd., Chiba, Japan. He has been engaged in research and development of optical modulators.

Junichiro Ichikawa received the B.S. and M.S. degrees in mineralogy from the University of Tokyo, Tokyo, Japan, in 1987 and 1989, respectively.

He joined the Optoelectronics Division of Sumitomo Osaka Cement Co., Ltd., in 1989 and engaged in research and development of ferroelectric material-based devices.

Ryo Shimizu received the B.E. and M.E. degrees in electronics from Toyo University, Tokyo, Japan, in 1996 and 1998, respectively.

In 1998, he joined Optoelectronics Research Division, New Technology Research Laboratories, Sumitomo Osaka Cement Co., Ltd., Chiba, Japan. He has been engaged in research and development of optical modulators.

Naokatsu Yamamoto received the Ph.D. degree in electrical engineering from Tokyo Denki University, Tokyo, Japan, in 2000.

From 2001, he joined the Communications Research Laboratory (now the National Institute of Information and Communications Technology, NICT), where he is currently the associate director general of Photonic ICT Research Center, and also the director of Advanced ICT Device Laboratory in NICT. He was also with Tokyo Denki University as a Visiting Professor from 2013 and the Ministry of Internal Affairs and Communications as a Deputy Director from 2012 to 2013. He engages in research including quantum dot photonic devices, a heterogeneous integration technology for convergence of photonics and electronics and developing a novel optical and electrical frequency resource for a dedicated moderate range communication as an access network.

Kouichi Akahane received B.E., M.E., and Ph.D degrees in Materials Science from the University of Tsukuba in 1997, 1999, and 2002, respectively.

He joined the Communications Research Laboratory (from April 1, 2004, National Institute of Information and Communications Technology), Koganei, Tokyo, in 2002. He is now a Director of Optical Access Technology Laboratory at the National Institute of Information and Communications Technology and is currently working on semiconductor photonic devices.

Atsushi Kanno (Senior member, IEEE) received the B. Sci., M. Sci., and Ph.D. degrees in science from the University of Tsukuba, Japan, in 1999, 2001, and 2005, respectively.

In 2005, he worked with the Venture Business Laboratory at the Institute of Science and Engineering at the University of Tsukuba. In 2006, he joined the National Institute of Information and Communications Technology (NICT), Japan. Since August 2022, he has worked with the Nagoya Institute of Technology, Japan. His research interests include microwave photonics, broadband optical and radio communication systems, sensing applications, and automotive network technologies.

Prof. Kanno is a member of the Institute of Electronics, Information, and Communication Engineers (IEICE), Japan Society of Applied Physics (JSAP), Laser Society of Japan, SPIE, and IEEE.

Tetsuya Kawanishi (Fellow, IEEE) received the B.E., M.E., and Ph.D. degrees in electronics from Kyoto University, Kyoto, Japan, in 1992, 1994, and 1997, respectively.

From 1994 to 1995, he was with the Production Engineering Laboratory of Panasonic. During 1997, he was with Venture Business Laboratory, Kyoto University, Kyoto, Japan, where he was engaged in research on electromagnetic scattering and near-field optics. In 1998, he joined the Communications Research Laboratory, Ministry of Posts and Telecommunications (now the National Institute of Information and Communications Technology), Tokyo, Japan. In 2004, he was a Visiting Scholar with the Department of Electrical and Computer Engineering, University of California at San Diego, San Diego, CA, USA. Since April 2015, he has been a Professor with Waseda University, Tokyo, Japan. His current research interests include high-speed optical modulators and RF photonics.

Prof. Kawanishi is the Chair of the Task Group on Fixed Wireless and Ground-Based Radar Systems (TG-FWS/GBRS) in Asia Pacific Telecommunity Wireless Group (AWG).